Iranian Journal of Fuzzy Systems

Volume 23, Number 4, (2026), pp. 75-95

Original paper

University of Sistan and Baluchestan

Fuzzy simulation of heat transfer in ternary hybrid nanofluid flow across a moving wedge

B. Amudha [1], M. Shanmugapriya [2], R. Sundareswaran [3] and Said Broumi [4]

[1,2,3] *Department of Mathematics, Sri Sivasubramaniya Nadar College of Engineering, Chennai, India.*
[4] *Laboratory of Information Processing, Faculty of Science Ben M'Sik, University of Hassan II, Casablanca, Morocco.*

amudha2350596@ssn.edu.in, shanmugapriyam@ssn.edu.in, sundareswaranr@ssn.edu.in, s.broumi@flbenmsik.ma

Abstract

This study investigated the impact of fuzzy nanoparticle volume fraction on the heat transport of ternary hybrid nanofluid (THNF) over a moving wedge, considering factors such as magnetic field, thermal radiation, and shape factor. The governing nonlinear coupled partial differential equations are transformed into ordinary differential equations using a suitable similarity transformation. The reformulated ordinary differential equations are then converted into fuzzy differential equations by utilizing the α-cut technique. The shooting method is employed to perform a numerical simulation via MATLAB. The present study reveals that the THNF exhibits a significantly enhanced heat transfer rate approximately 36.29% higher than the hybrid nanofluid, 59.30% higher than the nanofluid, and 69.87% higher than the base fluid. The volume fraction of nanoparticles in THNF may vary due to factors like inconsistencies during synthesis, particle aggregation, and dispersion stability, leading to uncertainty in predicting fluid behavior. To address this uncertainty, a fuzzy logic approach is employed. In the present study, triangular and trapezoidal fuzzy numbers are used to represent the nanoparticle volume fraction in THNF. By employing the technique in conjunction with the associated membership functions, the impact of these fuzzy parameters on different shape factors is systematically analyzed. The findings reveal that the blade-shaped nanoparticle exhibits higher heat transport than the other nanoparticle shapes.

Keywords: Magnetohydrodynamic, ternary hybrid nanofluid, shape effect, thermal radiation, triangular fuzzy number, trapezoidal fuzzy number.

1 Introduction

Improving heat transfer is crucial in various engineering applications, such as cooling systems, energy production, electronics, and renewable energy technologies. Nanofluid (NF) for enhancing thermal properties by adding nanoparticles into base fluid (BF) like water, ethylene glycol, and oils. The idea of improving thermal conductivity by adding solid particles to fluid was first proposed by Maxwell [25] in 1873. However, challenges like sedimentation, clogging, and erosion in flow channels emerged. In response, Masuda et al. [24] demonstrated that dispersing nanoparticles in a BF can enhance both the thermal conductivity and viscosity of liquids. Later, Choi and Eastman [9] expanded on Maxwell's model in 1995 by using nanometer-sized particles with larger surface area, which improved heat transport and suspension stability. They also noted that nanoparticles can flow smoothly through small channels without causing blockages. Numerous studies [7, 22, 31] have since confirmed that nanofluids exhibit better thermal conductivity than base fluid.

The next progression in this field is the development of hybrid nanofluids (HNF), which combines two or more types of nanoparticles to optimize both thermal conductivity and rheological properties, leading to even better heat transfer performance compared to BF. Alqahtani et al. [4] explored the Falkner-Skan flow of HNF over a moving wedge under

Corresponding Author: M. Shanmugapriya
Received: August 2025; Revised: April 2026; Accepted: July 2026.
https://doi.org/10.22111/ijfs.2026.52808.9330

convective boundary conditions. They applied a modified Buongiorno model to analyze ethylene glycol-water with molybdenum disulfide and silver nanoparticles considering joule heating, Lorentz force and radiation. Zainal et al. [37] investigated the impact of heat absorption, magnetic field, and suction effect on steady magnetohydrodynamic (MHD) flow in $(Al_2O_3 + Cu/H_2O)$ over permeable stretching/shrinking wedge using bvp4c MATLAB solver. Choudhary et al. [11] examined the heat transfer behavior of $(TiO_2 + CuO\ /\ H_2O)$ HNF flows past a moving wedge under the effects of magnetic field, thermal radiation, and a porous medium. They utilized a mass-based model to analyze their results. The heat and mass transport behavior of MHD HNF flow between two interconnected sheets under a magnetic field, viscosity, thermophoresis, and Brownian motion was done by Jalili et al. [18]. Rao et al. [30] investigated two dimensional (2-D) MHD flow of $(Al_2O_3 + Ag\ /\ H_2O)$ with first order boundary slip conditions over a porous stretching sheet. They solved using the Keller-Box numerical method.

To further optimize the thermal enhancement, THNF blends three different nano-sized particles in a base fluid. Varatharaj et al. [34] focused on optimizing heat transfer in Casson THNF $(Al_2O_3 + Ag + TiO_2\ /\ H_2O)$ on a stretched surface with slip effect and thermal radiation. They solved numerically combined Runge -Kutta and Keller-Box methods. Raji et al. [28] investigated the boundary layer flow over a porous wedge for THNF under the influence of a constant transverse magnetic field and heat radiation. Shanmugapriya et al. [33] explored the heat transport enhancement of THNF$(Cu + Al_2O_3 + MWCNT\ /\ H_2O)$ of different nanoparticle shapes through a magnetized stretching curved surface with thermal radiation effects. Some researchers [3, 14] have studied the THNF over a wedge.

In the modeling and solution of differential equations (DEs), various physical complexities such as geometrical configurations, variable coefficients, system parameters, and boundary conditions are critical. However, in practical scenarios, these factors are subject to uncertainties arising from measurement inaccuracies, experimental errors, and mechanical imperfections. This is where fuzzy set theory (FST) comes in. It allows us to deal with these uncertainties in a way that classical methods can't. While traditional models assume everything is exact and clear-cut, fuzzy sets recognize that things are so simple. Instead of saying something either fully belongs or doesn't belong to a set, fuzzy sets let us describe degrees of membership, making it easier to work with uncertainties. This flexibility is useful when we use fuzzy differential equations (FDE's), which helps in controlling fuzziness. The idea behind fuzzy sets was first introduced by Lotfi Zadeh [36] in 1965, and later expanded by Chang and Zadeh [10] with fuzzy numbers, followed by generalizations by Dubois and Prade [13]. Several studied have included fuzzy logic into nanofluids analyses. Al-Saedi et al. [5] investigated Jeffery-hamel flow by adding nanoparticles into the base fluid and treated volume fraction as an uncertain parameter. Their study introduces the Homotopy Analysis Method (HAM) for analyzing fuzzy velocity profiles. The impact of thermal radiation on the micropolar hybrid nanofluid flow between porous channel walls are examined by Kumar et al. [23]. They explored the uncertain effects on fuzzy velocity, microrotation and temperature profiles. Ayub et al. [6] studied the fluid flow in a vertical duct under uncertain conditions on cross hybrid nanofluid. They found that the effects of magnetic field, viscosity and nanoparticle volume fraction influence flow behavior and thermal characteristics. Shanmugapriya et al. [32] analyzed casson hybrid nanofluid over a moving wedge with chemical reactions under a fuzzy environment. Their results showed that hybrid nanofluids improve heat transfer compared to single nanofluids. Zulquarnain et al. [39] studied tri-hybrid Maxwell nanofluid flow a Riga wedge using fuzzy volume fractions. They analyzed the effects of porosity, nonlinear convection, and triangular fuzzy numbers on velocity and temperature distributions. Deepa et al. [12] examined blood-based Sisko ternary hybrid nanofluid flow over a stretching cylinder, using fuzzy triangular numbers to model nanoparticle volume fraction. It highlights the effect of magnetic field, cylinder curvature and chemical reactions in velocity, temperature and concentration profiles.

These investigations highlight the usefulness of fuzzy logic in modelling the uncertain nanoparticle volume fraction. However, these existing studies are restricted to channel flow, plane, vertical duct, wedge and Riga wedge flows. These works mostly deal with nanofluid or hybrid nanofluid with non-Newtonian fluid and do not consider ternary hybrid nanofluid in wedge flow. Even though fuzzy logic has been used before, to our knowledge, no study applies triangular and trapezoidal fuzzy numbers to ternary hybrid nanofluid over a wedge geometry. This gap creates the need for the present work.

1.1 Motivation

In this study, authors have focused on the impact of nanoparticle shapes on THNF, which consists of three different nanoparticle $Cu, Al_2O_3,$ and $MWCNT$ dispersed in base fluid H_2O. Research in this area can lead to improved thermal management systems and lead to new advancements in nanofluid based technologies. However, a thorough review of existing studies reveals a significant gap: no research has yet explored the behavior of THNF over a wedge in a fuzzy environment.

1.2 Objective

The authors of the present study examine the flow behavior of THNF over a wedge, considering key factors such as MHD and thermal radiation. A physical fluid flow model is developed, and through an appropriate similarity transformation, the partial differential equations (PDEs) are converted into a system of ordinary differential equations (ODEs). To handle uncertainties, FDE's are formulated using α-cut, triangular and trapezoidal fuzzy numbers. The shooting method in MATLAB is employed to solve the FDE's and the effects of the key parameters are visualized as 3-D plots.

1.3 Novelty

The novelty of the present work is

- The effects of magnetized THNF with different nanoparticle shapes over a moving wedge in a fuzzy environment have not been explored in previous research.
- In this study, the nanoparticle volume fraction for THNF are represented using triangular and trapezoidal fuzzy number, with the help of α-cut.
- A comparison of the effects between various nanoparticle shapes is made using fuzzy membership functions.

2 Basic definitions

This section introduces fundamental definitions and notations related to fuzzy systems, which will be utilized in subsequent computations.

Definition 1. [36] Let $\check{X}$ denote a universe of discourse and $\check{x}$ be any element of $\check{X}$. The Fuzzy set (F_{set}) $\check{\mathcal{F}}$ on $\check{X}$ is defined as a set of ordered pairs, $\check{\mathcal{F}} = \left\{(\check{x}, M_{\check{\mathcal{F}}}(\check{x})) \mid \check{x} \in \check{X}\right\}$ where $M_{\check{\mathcal{F}}}(\check{x}) : \check{X} \to [0,1]$ is called the membership function.

Definition 2. [36] For a F_{set} $\check{\mathcal{F}}$ defined on a universe $\check{X}$, the α-cut of $\check{\mathcal{F}}$, denoted by $\check{\mathcal{F}}_\alpha$ is: $\check{\mathcal{F}}_\alpha = \left\{\check{x} \in \check{X} \mid M_{\check{\mathcal{F}}}(\check{x}) \geq \alpha\right\}$, where $\alpha \in [0,1]$.

Definition 3. [27] A F_{set} $\check{\mathcal{F}}$ on $\mathbb{R}$ is said to be a Fuzzy number (F_{number}) if the following conditions are satisfied.

- $\check{\mathcal{F}}$ is a convex fuzzy set, i.e.,$\mu_{\tilde{A}}(\lambda\check{x}_1 + (1-\lambda)\check{x}_2) \geq \min\{\mu_{\tilde{A}}(\check{x}_1), \mu_{\tilde{A}}(\check{x}_2)\}$, for all $\check{x}_1, \check{x}_2 \in \mathbb{R}$ and $\lambda \in [0,1]$.
- $\check{\mathcal{F}}$ is normalized, i.e., there exists $\check{x}_0 \in \mathbb{R}$ such that $M_{\check{\mathcal{F}}}(\check{x}_0) = 1$ (here, $\check{x}_0$ is the mean value of $\check{\mathcal{F}}$).
- $M_{\check{\mathcal{F}}}(\check{x}_0)$ is piecewise continuous.
- The support of $\check{\mathcal{F}}$, i.e., supp($\check{\mathcal{F}}$), must be bounded.

Definition 4. [27] A Triangular Fuzzy Number ($TriF_{number}$) is represented by three real parameters $\check{\mathcal{F}} = \{i_1, i_2, i_3\}$, where $i_1 \leq i_2 \leq i_3$. It defines a F_{set} on the real line $\mathbb{R}$ with the membership function ($M_{\check{\mathcal{F}}}(\check{x})$) given by

$$M_{\check{\mathcal{F}}}(\check{x}) = \begin{cases} \frac{\check{x}-i_1}{i_2-i_1}, & \text{if } i_1 \leq \check{x} \leq i_2, \\ \frac{i_3-\check{x}}{i_3-i_2}, & \text{if } i_2 \leq \check{x} \leq i_3, \\ 0, & \text{otherwise.} \end{cases} \tag{1}$$

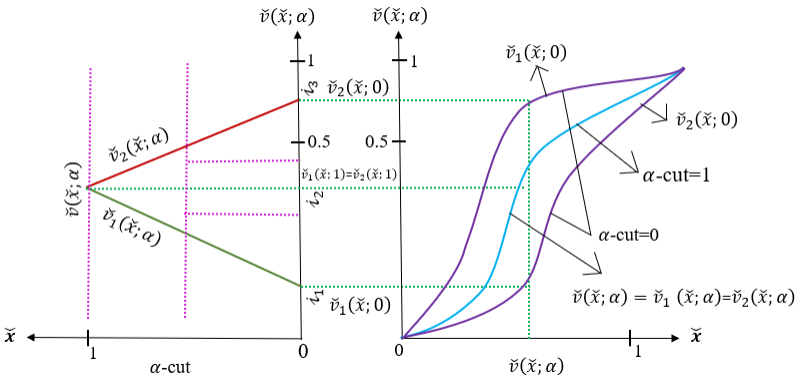

Figure 1: Membership function of $TriF_{number}$

Here, i_1, i_2 and i_3 denotes the lower limit, the modal value, and the upper limit of the F_{number}, respectively, and, it is illustrated in Figure 1.

Definition 5. [27] A Trapezoidal Fuzzy Number ($TrapF_{number}$) denoted by $\check{\mathcal{F}}$ is defined as $\{i_1, i_2, i_3, i_4\}$ where $i_1 \leq i_2 \leq i_3 \leq i_4$. It represents a F_{set} on $\mathbb{R}$ with the $M_{\check{\mathcal{F}}}(\check{x})$ defined as

$$M_{\check{\mathcal{F}}}(\check{x}) = \begin{cases} 0, & \check{x} < i_1 \\ \dfrac{\check{x} - i_1}{i_2 - i_1}, & i_1 \leq \check{x} \leq i_2 \\ 1, & i_2 \leq \check{x} \leq i_3 \\ \dfrac{i_4 - \check{x}}{i_4 - i_3}, & i_3 \leq \check{x} \leq i_4 \\ 0, & \check{x} > i_4 \end{cases} \tag{2}$$

Here, i_1 and i_3 denote the lower and upper bounds, respectively, while the interval $[i_2, i_4]$ represents the region where the membership value is equal to 1 and, it is illustrated in Figure 2.

Figure 2: Membership function of $TrapF_{number}$

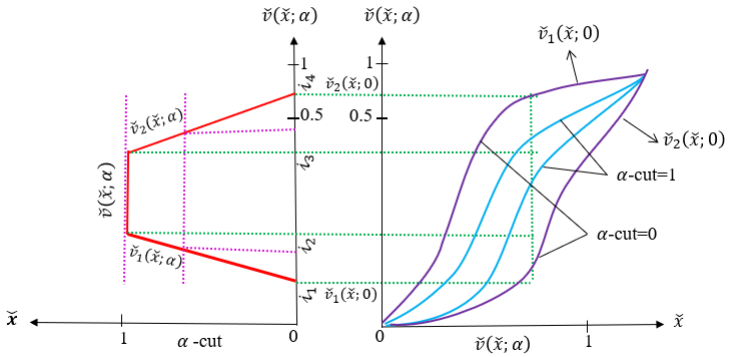

Definition 6. [32] Let $\check{I}$ be a real interval. A function $\check{v} : \check{I} \to \check{\mathcal{F}}$ is called a Fuzzy process ($F_{process}$), denoted as $\check{v}(\check{x}; \alpha)$. It is defined by $\check{v}(\check{x}; \alpha) = [i_1^{\alpha}, i_3^{\alpha}]$, $\check{x} \in \hat{I}$, $\alpha \in [0, 1]$. The derivative of a $F_{process}$ $\check{v}(\check{x}; \alpha)$ with respect to $\check{x}$, denoted by $\frac{d\check{v}(\check{x};\alpha)}{d\check{x}}$, is also a F_{set} and is defined as $\frac{d\check{v}(\check{x};\alpha)}{d\check{x}} = \left[\frac{di_1^{\alpha}}{d\check{x}}, \frac{di_3^{\alpha}}{d\check{x}}\right]$.

Definition 7. [32] Let $\check{I} \subseteq \mathbb{R}$ and $\hat{v}$ be a fuzzy-valued function on $\check{I}$. Let $\check{v}(\check{x}; \alpha) = [i_1^{\alpha}, i_3^{\alpha}]$ for all α-cuts. Assume that i_1^{α} and i_3^{α} have continuous derivatives and are differentiable for all $\check{x} \in \hat{I}$ and $\alpha \in [0, 1]$. Then, the derivative of the fuzzy-valued function is defined as $\left[\frac{d\check{v}(\check{x};\alpha)}{d\check{x}}\right]_{\alpha} = \left[\frac{di_1^{\alpha}}{d\check{x}}, \frac{di_3^{\alpha}}{d\check{x}}\right]_{\alpha}$. Similarly, higher-order derivatives can be defined in the same manner. A F_{number} represented as an ordered pair of functions $\left[\frac{d\check{v}(\check{x};\alpha)}{d\check{x}}\right]_{\alpha}$ satisfies the following conditions:

i. $\frac{di_1^{\alpha}}{d\check{x}}$ and $\frac{di_3^{\alpha}}{d\check{x}}$ are continuous in $[0, 1]$.

ii. $\frac{di_1^{\alpha}}{d\check{x}}$ is an increasing function on $[0, 1]$.

iii. $\frac{di_3^{\alpha}}{d\check{x}}$ is a decreasing function on $[0, 1]$.

iv. $\frac{di_1^{\alpha}}{d\check{x}} \leq \frac{di_3^{\alpha}}{d\check{x}}$ on $[0, 1]$.

3 Mathematical formulation

An incompressible 2-D steady MHD flow of a THNF over a moving wedge is considered. The study incorporates for the combined effects of thermal radiation and nanoparticle shape factor on heat transfer performance, as illustrated in the Figure 3. The flow field is described by the velocity components (u, v) in the x and y directions, respectively.

The velocity of the stretching wedge is defined as $u_w(x) = U_w x^m$, while the external free stream velocity is given by $u_e(x) = U_\infty x^m$. The parameter $m = \beta/(2-\beta)$ corresponds to the Hartree pressure gradient. A uniform magnetic field B_0 is applied along the x-axis direction, influencing the electrically conducting THNF. The wall temperature T_w is assumed to be higher than the ambient fluid temperature T_∞, resulting in heat transfer from the surface into the fluid. To account for thermal radiation effects, the Rosseland approximation is adopted, which is appropriate for optically thick media. According to this approximation, the radiative heat flux q_r is given by:

$$q_r = -\frac{4\sigma^*}{3k^*}\frac{\partial T^4}{\partial y},$$

where σ^* is the Stefan-Boltzmann constant, k^* is the mean absorption coefficient, and T represents the local fluid temperature within the boundary layer. To linearize the nonlinear term T^4, a Taylor series expansion is carried out about the ambient temperature T_∞. By neglecting higher-order terms, the expression is simplified to obtain:

$$T^4 \approx 4T_\infty^3 T - 3T_\infty^4.$$

Substituting this approximation into the radiative heat flux expression yields:

$$q_r = -\frac{16\sigma^* T_\infty^3}{3k^*}T_y.$$

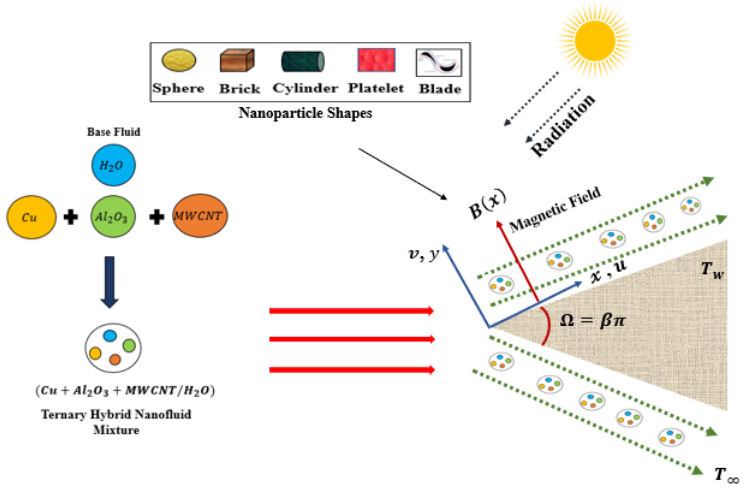

Figure 3: Schematic flow diagram

3.1 Governing equations

The fundamental governing equations describing the flow and heat transport behavior of this THNF are based on the formulation introduced by Mishra et al. [26] and Amar et al. [2].

$$u_x + v_y = 0, \tag{3}$$

$$uu_x + vu_y = u_e\frac{du_e}{dx} + \frac{\mu_{\mathrm{THNF}}}{\rho_{\mathrm{THNF}}}u_{yy} + \frac{\sigma_{\mathrm{BF}}B^2}{\rho_{\mathrm{THNF}}}(u_e - u), \tag{4}$$

$$uT_x + vT_y = \frac{k_{\mathrm{THNF}}}{(\rho C_p)_{\mathrm{THNF}}}T_{yy} - \frac{1}{(\rho C_p)_{\mathrm{THNF}}}\frac{\partial q_r}{\partial y}. \tag{5}$$

The imposed boundary constraints are

$$\begin{cases} u = u_w(x) = U_w x^m, & v = 0, \quad T = T_w & \text{at } y = 0, \\ u = u_e(x) = U_\infty x^m, & T = T_\infty & \text{as } y \to \infty. \end{cases} \tag{6}$$

Table 1: Physicochemical traits of Base fluid and Nanoparticles [15, 19]

Properties	H_2O	Cu	Al_2O_3	$MWCNT$
C_p (J/kg·K)	4179	385	765	796
k (W/m·K)	0.613	400	40	3000
ρ (kg/m^3)	997.1	8933	3970	1600

3.2 Special features of THNF $(Cu + Al_2O_3 + MWCNT\ /\ H_2O)$

The physicochemical properties of the THNF are summarized in Table 1, while their corresponding mathematical formulations are provided in Eq. (7) [1, 20].
The thermophysical properties of THNF are given by

$$\begin{cases} \mu_{\text{THNF}} & = \mu_{\text{BF}}(1-\varphi_{Cu})^{-2.5}(1-\varphi_{Al_2O_3})^{-2.5}(1-\varphi_{MWCNT})^{-2.5} \\ \rho_{\text{THNF}} & = (1-\varphi_{Cu})\Big\{(1-\varphi_{Al_2O_3})\big[(1-\varphi_{MWCNT})\rho_{\text{BF}} + \varphi_{MWCNT}\rho_{MWCNT}\big] \\ & \quad + \varphi_{Al_2O_3}\rho_{Al_2O_3}\Big\} + \varphi_{Cu}\rho_{Cu} \\ k_{\text{THNF}} & = k_{\text{HNF}} \cdot \left(\dfrac{k_{Cu} + (n-1)k_{\text{HNF}} - (n-1)\varphi_{Cu}(k_{\text{HNF}} - k_{Cu})}{k_{Cu} + (n-1)k_{\text{HNF}} + \varphi_{Cu}(k_{\text{HNF}} - k_{Cu})}\right) \\ k_{\text{HNF}} & = k_{\text{NF}} \cdot \left(\dfrac{k_{Al_2O_3} + (n-1)k_{\text{NF}} - (n-1)\varphi_{Al_2O_3}(k_{\text{NF}} - k_{Al_2O_3})}{k_{Al_2O_3} + (n-1)k_{\text{NF}} + \varphi_{Al_2O_3}(k_{\text{NF}} - k_{Al_2O_3})}\right) \\ k_{\text{NF}} & = k_{\text{BF}} \cdot \left(\dfrac{k_{MWCNT} + (n-1)k_{\text{BF}} - (n-1)\varphi_{MWCNT}(k_{\text{BF}} - k_{MWCNT})}{k_{MWCNT} + (n-1)k_{\text{BF}} + \varphi_{MWCNT}(k_{\text{BF}} - k_{MWCNT})}\right) \\ (\rho C_p)_{\text{THNF}} & = (1-\varphi_{Cu})\Big\{(1-\varphi_{Al_2O_3})\big[(1-\varphi_{MWCNT})(\rho C_p)_{\text{BF}} \\ & \quad + \varphi_{MWCNT}(\rho C_p)_{MWCNT}\big] + \varphi_{Al_2O_3}(\rho C_p)_{Al_2O_3}\Big\} \\ & \quad + \varphi_{Cu}(\rho C_p)_{Cu} \end{cases} \tag{7}$$

The nanoparticle volume fractions of copper (Cu), aluminium oxide (Al_2O_3) and multi-walled carbon tube (MWCNT) are denoted as $\varphi_{Cu}, \varphi_{Al_2O_3}$ and φ_{MWCNT} respectively. The thermal conductivity of each nanoparticle is denoted by $k_{Cu}, k_{Al_2O_3}, k_{MWCNT}$ and k_{BF} for the base fluid. The thermal conductivity of HNF and NF is represented by k_{HNF} and k_{NF} respectively. The density of each nanoparticle is denoted by $\rho_{Cu}, \rho_{Al_2O_3}, \rho_{MWCNT}$ and ρ_{BF} for the base fluid. Similarly, the volumetric heat capacity of each nanoparticle is denoted by $(\rho C_p)_{Cu}, (\rho C_p)_{Al_2O_3}, (\rho C_p)_{MWCNT}$ and $(\rho C_p)_{\text{BF}}$ for the base fluid.
Here, μ_{THNF}, ρ_{THNF}, k_{THNF}, and $(\rho C_p)_{\text{THNF}}$ represent the dynamic viscosity, density, thermal conductivity, and volumetric heat capacity of the ternary hybrid nanofluid, respectively. The shape factor (n) represents the influence of nanoparticle geometry on the nanofluid's flow, their impact on thermal conductivity and heat transfer. The different shapes of nanoparticle conduct heat and interact with the fluid in distinct ways. Here $n = 3, 3.6, 4.9, 5.7$ and 8.6 represents sphere, brick, cylinder, platelet and blade shaped nanoparticle.

3.3 Expressing the governing equation in dimensionless form

The physical model is simplified using the following similarity transformations, as adopted in the studies by Jabeen et al. [17] and Zeeshan et al. [38]. The similarity variable ζ and stream function ψ are defined as:

$$\psi = \left[\frac{2\vartheta_{\text{BF}}U_\infty x^{m+1}}{m+1}\right]^{1/2} f(\zeta), \quad \zeta = \left[\frac{(m+1)U_\infty}{2\vartheta_{\text{BF}}}\right]^{1/2} x^{\frac{m-1}{2}} y, \quad \theta(\zeta) = \frac{T - T_\infty}{T_w - T_\infty}. \tag{8}$$

Using the similarity transformations, the velocity components u and v are expressed as:

$$u = \frac{\partial \psi}{\partial y} = U_\infty x^m f'(\zeta), \tag{9}$$

$$v = -\frac{\partial \psi}{\partial x} = -\left[\frac{(m+1)\vartheta_{\text{BF}}U_\infty x^{m-1}}{2}\right]^{1/2} \left[f(\zeta) + \zeta\frac{(m-1)}{(m+1)}f'(\zeta)\right]. \tag{10}$$

Substituting the above similarity transformations into the governing equations (Eqs. (3), (4) and (5)) and applying the boundary layer approximations, the system of PDEs is reduced to a set of coupled nonlinear ODEs, as given in

Eq. (11) and (12).

$$f''' - \Delta_1\Delta_2\left[\frac{2m}{m+1}(f'^2-1) - ff''\right] + \Delta_1 M\left(\frac{2}{m+1}\right)(1-f') = 0, \tag{11}$$

$$\theta''\left(1+\frac{R}{\Delta_4}\right) - \frac{\Pr\Delta_3}{\Delta_4}\left(\frac{4m}{m+1}f'\theta - f\theta'\right) = 0. \tag{12}$$

The employed boundary conditions are

$$f(0)=0, \quad f'(0)=\gamma, \quad \theta(0)=1, \quad f'(\infty)=1, \quad \theta(\infty)=0. \tag{13}$$

The non-dimensional parameters used in Eqs. (11)–(13) are defined as follows: Magnetic parameter: $M = \frac{\sigma B_0^2}{\rho_{\mathrm{BF}} U_\infty}$, Radiation parameter: $R = \frac{16\sigma^* T_\infty^3}{3k^* k_{\mathrm{BF}}}$, Prandtl number: $\Pr = \frac{\vartheta_{\mathrm{BF}}(\rho C_p)_{\mathrm{BF}}}{k_{\mathrm{BF}}}$, Moving wedge parameter: $\gamma = \frac{U_w}{U_\infty}$. And the thermal parameters

$$\begin{aligned}
&\Delta_1 = (1-\varphi_{Cu})^{-2.5}(1-\varphi_{Al_2O_3})^{-2.5}(1-\varphi_{MWCNT})^{-2.5},\\
&\Delta_2 = (1-\varphi_{Cu})\big\{(1-\varphi_{Al_2O_3})\big[(1-\varphi_{MWCNT})\rho_{\mathrm{BF}} + \varphi_{MWCNT}\rho_{MWCNT}\big] + \varphi_{Al_2O_3}\rho_{Al_2O_3}\big\} + \varphi_{Cu}\rho_{Cu},\\
&\Delta_3 = (1-\varphi_{Cu})\big\{(1-\varphi_{Al_2O_3})\big[(1-\varphi_{MWCNT})(\rho C_p)_{\mathrm{BF}} + \varphi_{MWCNT}(\rho C_p)_{MWCNT}\big] + \varphi_{Al_2O_3}(\rho C_p)_{Al_2O_3}\big\},\\
&\qquad + \varphi_{Cu}(\rho C_p)_{Cu},\\
&\Delta_4 = \frac{k_{\mathrm{THNF}}}{k_{\mathrm{BF}}}.
\end{aligned}$$

3.4 Important quantities of engineering interest

In the context of THNF flow and heat transfer, the skin friction factor (Sf_x) and the Nusselt number (Nu_x) are critical parameters. The expressions for these quantities are expressed as follows [17] :

$$Sf_x = \frac{2\tau_w}{\rho_{BF}U_e^2}, \quad Nu_x = \frac{xq_w}{k_{BF}(T_w - T_\infty)}, \tag{14}$$

where; τ_w and q_w stand for wall shear stress and the heat flux, respectively.

$$\tau_w = \mu_{\mathrm{THNF}}\left.\frac{\partial u}{\partial y}\right|_{y=0}, \quad q_w = -\left[k_{\mathrm{THNF}}\left.\frac{\partial T}{\partial y}\right|_{y=0} + \frac{16\sigma^* T_\infty^3}{3k^*}\left.\frac{\partial T}{\partial y}\right|_{y=0}\right]. \tag{15}$$

Using the similarity transformations and temperature relation (Eq. (8)) along with the velocity component u (Eq. (9)) into the wall quantity definitions (Eq. (15)), the expressions are transformed into the dimensionless forms given below.

$$Sf_x = \frac{2\mu_{\mathrm{THNF}}\, x^{\frac{3m-1}{2}}\, f''(0)\sqrt{\frac{U_\infty(m+1)}{2\vartheta_{\mathrm{BF}}}}}{\rho_{\mathrm{BF}}\, U_\infty^2\, x^{2m}}. \tag{16}$$

$$Nu_x = -\frac{k_{\mathrm{THNF}}}{k_{\mathrm{BF}}}\sqrt{\frac{m+1}{2}}\left(1+\frac{R}{\Delta_4}\right)\sqrt{\frac{U_\infty x^{m+1}}{\vartheta_{\mathrm{BF}}}}\,\theta'(0). \tag{17}$$

After simplification and by introducing the local Reynolds number $\mathrm{Re}_x = \frac{u_e(x)x}{\vartheta_{\mathrm{BF}}}$, the expression can be written in the following non-dimensional form:

$$Sf_x\,\mathrm{Re}_x^{0.5} = \frac{1}{(1-\varphi_{Cu})^{-2.5}(1-\varphi_{Al_2O_3})^{-2.5}(1-\varphi_{MWCNT})^{-2.5}}\sqrt{\frac{m+1}{2}}2f''(0). \tag{18}$$

$$Nu_x\mathrm{Re}_x^{-0.5} = -\frac{k_{\mathrm{THNF}}}{k_{BF}}\sqrt{\frac{m+1}{2}}\left(1+\frac{R}{\Delta_4}\right)\theta'(0). \tag{19}$$

4 Solution methodology

In the present study, a numerical approach is employed to solve the nonlinear boundary value problem (BVP) arising from the governing equations. Such problems are generally difficult to handle analytically due to their nonlinear and coupled nature. Therefore, an efficient numerical technique is required to obtain accurate solutions.
The shooting method converts the BVP into an initial value problem (IVP). In this approach, the unknown boundary conditions at the initial point are estimated and iteratively refined so that the boundary conditions at infinity are satisfied. A Newton-Raphson iteration scheme is used to update the guessed values and ensure convergence of the solutions. To apply the shooting method, the system of equations are reduced to a set of first-order ODEs using variable substitutions as follows: $f = l_1, \quad f' = l_2, \quad f'' = l_3, \quad \theta = l_4, \quad \theta' = l_5$.
Using the above transformations, the governing equations from Eq. (11) to Eq. (13) are reduced to coupled system of first-order differential equations, as presented in Eq. (20) and (21) .

$$l_3' = \Delta_1\Delta_2\left[\frac{2m}{m+1}(l_2^2 - 1) - l_1 l_3\right] - \Delta_1 M\left(\frac{2}{m+1}\right)(1 - l_2), \tag{20}$$

$$l_5' = \frac{\Pr}{1 + R/\Delta_4} \cdot \frac{\Delta_3}{\Delta_4}\left[\frac{4m}{m+1} l_2 l_4 - l_1 l_5\right]. \tag{21}$$

The corresponding boundary conditions are expressed as:

$$\begin{aligned} &l_1(0) = 0, \quad l_2(0) = \gamma, \quad l_3(0) = a_1, \quad l_4(0) = 1, \quad l_5(0) = a_2, \\ &l_2(\infty) = 1, \quad l_4(\infty) = 0. \end{aligned} \tag{22}$$

Here, a_1 and a_2 represent the unknown initial conditions that must be determined. The unknown initial guesses a_1 and a_2 are iteratively adjusted using the Newton-Raphson method. For each set of guessed values, the system of differential equations is integrated numerically over the domain $0 \le \zeta \le \zeta_\infty$. The computed values at ζ_∞ are the compared with the prescribed boundary conditions. The iteration process continues until the maximum error between computed and required boundary conditions is less than 10^{-6}, ensuring convergence.

Pseudo Code: Shooting method

Step 1: Define parameters and domain $\zeta \in [0, \zeta_\infty]$.
Step 2: Convert governing equations into first-order ordinary differential equations.
Step 3: Assign known boundary conditions and guess unknown initial values a_1 and a_2 .
Step 4: Solve the ODE system numerically.
Step 5: Compute residual errors at $\zeta = \zeta_\infty$.
Step 6: Update guesses using Newton-Raphson method.
Step 7: Repeat Steps 4-6 until convergence $\max(|R_i|) < 10^{-6}$.
Step 8: Evaluate: $Sf_x = l_3(0), Nu_x = -l_5(0)$.

After achieving convergence, the physical quantities of interest are obtained from the wall derivatives as: $Sf_x = f''(0) = l_3(0), Nu_x = \theta'(0) = -l_5(0)$. These values are directly extracted from the numerical solution at $\zeta = 0$ and are used to analyze the skin friction and heat transfer characteristics.

4.1 Validation

To verify the accuracy of our numerical solution, Tables 2 and 3 present the value of the skin friction factor (Sf_x) and Nusselt number (Nu_x) for the base fluid ($\varphi_{Cu} = \varphi_{Al_2O_3} = \varphi_{MWCNT} = 0$) with the magnetic parameter $M = 0$, and for various values of m. The slight deviations observed in the Homotopy Perturbation Method (HPM) results are due to the inherent approximate nature of the perturbation series. However, the numerical shooting method shows excellent agreement with existing results, confirming the accuracy of the present mathematical model.

Table 2: Comparison of $f''(0)$ at selected values of m when $M = \varphi_{Cu} = \varphi_{Al_2O_3} = \varphi_{MWCNT} = 0$ and Pr = 6.2.

m	Yacob et al. [35]	Ibrahim et al. [16]	Chakraborty et al. [8]	Present Results Shooting	Present Results HPM
0	0.4696	0.469600	0.469600	0.469600	0.458334
1/11	0.6550	0.654994	0.654993	0.654994	0.666666
1/5	0.8021	0.802125	0.802125	0.802125	0.875000
1/3	0.9277	0.927680	0.927680	0.927680	1.083333
1/2	1.0389	1.038900	1.038900	1.038900	1.291666
1	1.2326	1.232587	1.232587	1.232587	1.708333

Table 3: Comparison of $\theta'(0)$ at selected values of Pr when $m = M = \varphi_{Cu} = \varphi_{Al_2O_3} = \varphi_{MWCNT} = 0$.

Pr	Khan and Pop [21]	Raju et al. [29]	Gopi Krishna and Shanmugapriya [22]	Present Results Shooting	Present Results HPM
0.72	0.4184	0.4181	0.4181	0.4184	0.4233
1	0.4696	0.4696	0.4696	0.4696	0.4583
2	0.5972	0.5972	0.5972	0.5972	0.5833
3	0.6860	0.6860	0.6860	0.6860	0.7083
6	0.8673	0.8673	0.8673	0.8673	1.0833
10	1.0297	1.0297	1.0297	1.0297	1.5833

4.2 Translating the crisp problem into a fuzzy problem through fuzzy differential equations

Even small variations in the volume fraction of the nanoparticle can influence the velocity and temperature in fluid flow problems. In many studies, the volume fraction of nanoparticles is typically considered within the range of 0.01 to 0.04. Since the fluid flow behavior depends on these specific crisp values, any uncertainty arising from fixing these values can affect the results. Fuzzy logic helps to reduce this uncertainty by considering a range of possible values instead of just one. So, when dealing with complex heat transfer problems, it is useful to treat the nanoparticle volume fractions as F_{number}. In this study, the volume fraction of nanoparticles is treated as $TriF_{number}$ [0, 0.05, 0.1] and a $TrapF_{number}$ [0, 0.05, 0.1, 0.15], as shown in Table 4. To handle these F_{number}, the α-cut technique is used, which helps convert the equations into fuzzy differential equations (FDEs).The converted FDEs are

$$f'''(\zeta,\alpha) - \Delta_1\Delta_2\left(\frac{2m}{m+1}(f'(\zeta,\alpha)^2 - 1) - f(\zeta,\alpha)f''(\zeta,\alpha)\right) + \Delta_1 M\left(\frac{2}{m+1}\right)(1 - f'(\zeta,\alpha)) = 0, \tag{23}$$

$$\theta''(\zeta,\alpha)\left(1 + \frac{R}{\Delta_4}\right) - \frac{\Pr\Delta_3}{\Delta_4}\left[\frac{4m}{m+1}f'(\zeta,\alpha)\theta(\zeta,\alpha) - f(\zeta,\alpha)\theta'(\zeta,\alpha)\right] = 0. \tag{24}$$

The boundary conditions are

$$\begin{cases} f(\zeta,\alpha) = 0, \quad f'(\zeta,\alpha) = \gamma, \quad \theta(\zeta,\alpha) = 1 & \text{at } \zeta = 0 \\ f'(\zeta,\alpha) = 1, \quad \theta(\zeta,\alpha) = 0 & \text{as } \zeta \to \infty \end{cases} \tag{25}$$

Here, the fuzzy velocity profile is $f'(\zeta,\alpha) = \left[\underline{f'}(\zeta,\alpha), \overline{f'}(\zeta,\alpha)\right]$, where $\underline{f'}(\zeta,\alpha)$ is the lower bound and $\overline{f'}(\zeta,\alpha)$ is the upper bound of the velocity profile. Similarly, $\theta(\zeta,\alpha) = \left[\underline{\theta}(\zeta,\alpha), \overline{\theta}(\zeta,\alpha)\right]$ represents the fuzzy temperature profile.

Table 4: $TriF_{number}$ and $TrapF_{number}$ values for fuzzy nanoparticle volume fraction

Fuzzy Number	**Crisp Value**	$TriF_{number}$	**α-cut**	$TrapF_{number}$	**α-cut**
φ_{Cu}, $\varphi_{Al_2O_3}$, φ_{MWCNT}	[0.01–0.04]	[0, 0.05, 0.1]	$[0.05\alpha, 0.1 - 0.05\alpha]$	[0, 0.05, 0.1, 0.15]	$[0.05\alpha, 0.15 - 0.05\alpha]$

Here, $\alpha \in [0,1]$ denotes the level of membership in the α-cut representation. The $TriF_{number}$ and $TrapF_{number}$ defines the uncertainty range of the nanoparticle volume fraction at different α-levels.

5 Results and discussion

In this section, graphical illustrations of dimensionless parameters, extracted from the numerically obtained solutions, are utilized to examine the effects of various physical factors on the flow dynamics of the THNF via 3-D plots. For the numerical simulation, the ranges for the control parameters were selected based on existing literatures [3], [18], [20]: $0.1 \leq m \leq 1$, $1 \leq M \leq 3$, $0.5 \leq R \leq 2$, $0.72 \leq \Pr \leq 10$, $0.1 \leq \gamma \leq 0.7$, $0.01 \leq \varphi_{Cu}, \varphi_{Al_2O_3}, \varphi_{MWCNT} \leq 0.15$, $3 \leq n \leq 8.6$. The dimensionless parameters are examined within a defined numerical interval so that the analysis represents conditions commonly encountered in practical applications. These intervals are selected to achieve a balance between physical realism and computational practicality. By using suitable parameter limits, the model can accurately represent the behavior of the system while maintaining numerical stability and efficiency. Extremely large or small parameter values may cause instability or divergence, leading to unreliable outcomes. Therefore, the chosen ranges for the non-dimensional parameters are aligned with findings from previous experimental and theoretical studies to ensure the validity and consistency of the results. The fixed values of the parameters are taken as: $m = 0.5$, $M = 1.5$, $R = 1$, $\Pr = 6.2$, $\gamma = 0.5$, $\varphi_{Cu} = \varphi_{Al_2O_3} = \varphi_{MWCNT} = 0.05$, $n = 8.6$. The 3D plots illustrate the relationship between the parameters $m, M, R, \Pr, \varphi_{Cu} = \varphi_{Al_2O_3} = \varphi_{MWCNT} = 0$ and the skin friction coefficient and Nusselt number. Figure 4 depicts the influence of the Hartree pressure gradient parameter (m) and magnetic field parameter (M) on $f''(0)$. It is observed that both m and M exhibit an increasing trend within the range $0.1 \leq m \leq 1$ and $1 \leq M \leq 2$. As the velocity of the fluid particles increases, both m and M contribute to an upward trend in the skin friction coefficient.

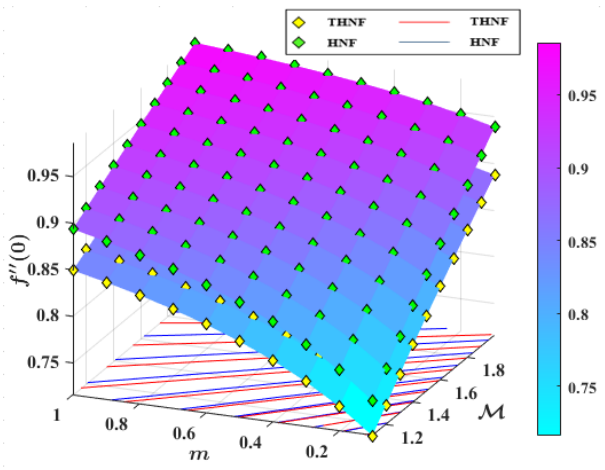

Figure 4: Impact of m and M on $f''(0)$.

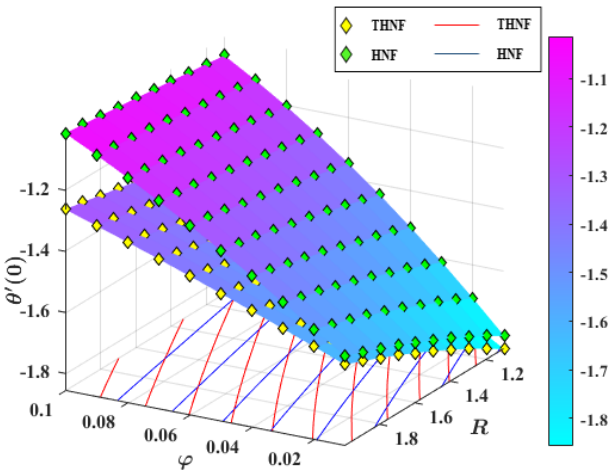

Figure 5: Impact of R and φ on $\theta'(0)$.

Figure 5 displays the impact of the radiation parameter (R) and the total nanoparticle volume fraction ($\varphi = \varphi_{Cu} + \varphi_{Al_2O_3} + \varphi_{MWCNT}$) on the Nusselt number component $\theta'(0)$, which shows an increasing trend. As both R and φ increase, $\theta'(0)$ exhibits a higher rate of change, indicating their significant influence on thermal transport characteristics. The influence of the Prandtl number (Pr) and nanoparticle volume fraction (φ) on $\theta'(0)$ is illustrated in Figure 6. An increasing trend in $\theta'(0)$ is observed with rising values of Pr and φ, highlighting their impact on enhancing heat transfer rates. Table 5 provides the numerical results for Sf_x and Nu_x, corresponding to various flow parameters for the THNF, specifically $\mathrm{Cu} + \mathrm{Al_2O_3} + \mathrm{MWCNT/H_2O}$.

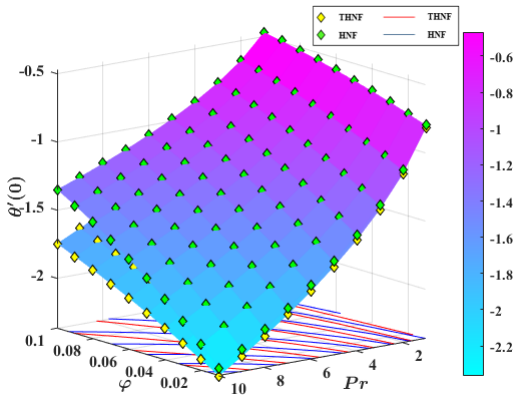

Figure 6: Behavior of f′(ζ) aganist $\tilde{\lambda}$

Table 5: Impact of THNF and HNF Parameters on Sf_x and Nu_x

m	M	γ	R	Pr	φ_{Cu}	$\varphi_{Al_2O_3}$	φ_{MWCNT}	n	THNF		HNF	
									Sf_x	Nu_x	Sf_x	Nu_x
0.1									0.7969	-1.0330	0.8410	-1.1783
0.3									0.8292	-1.2688	0.8745	-1.4474
0.5									0.8522	-1.4175	0.8983	-1.6173
0.7									0.8693	-1.5215	0.9161	-1.7361
	1								0.7834	-1.4090	0.8240	-1.6072
	1.5								0.8522	-1.4175	0.8983	-1.6173
	2								0.9159	-1.4251	0.9670	-1.6261
	2.5								0.9756	-1.4318	1.0313	-1.6339
		0.1							1.4434	-1.1505	1.5257	-1.2987
		0.3							1.1584	-1.2882	1.2227	-1.4630
		0.5							0.8522	-1.4175	0.8983	-1.6173
		0.7							0.5257	-1.5398	0.5535	-1.7629
			0.5						0.8522	-1.5126	0.8983	-1.7605
			1						0.8522	-1.4175	0.8983	-1.6173
			1.5						0.8522	-1.3393	0.8983	-1.5056
			2						0.8522	-1.2733	0.8983	-1.4154
				0.72					0.8522	-0.5264	0.8983	-0.6009
				1					0.8522	-0.6129	0.8983	-0.6995
				6.2					0.8522	-1.4175	0.8983	-1.6173
				10					0.8522	-1.7660	0.8983	-2.0155
					0.01				0.8544	-1.5582	0.9002	-1.7610
					0.05				0.8522	-1.4175	0.8983	-1.6173
					0.1				0.8427	-1.2751	0.8886	-1.4672
					0.15				0.8267	-1.1579	0.8719	-1.3405
						0.01			0.8784	-1.5364	0.9261	-1.7482
						0.05			0.8522	-1.4175	0.8983	-1.6173
						0.1			0.8181	-1.2934	0.8621	-1.4785
						0.15			0.7828	-1.1888	0.8244	-1.3601
							0.01		0.8890	-1.5726	–	–
							0.05		0.8522	-1.4175	–	–
							0.1		0.8067	-1.2625	–	–
							0.15		0.7621	-1.1360	–	–
								3	0.8522	-1.7072	0.8983	-1.8093
								4.9	0.8522	-1.5976	0.8983	-1.7374
								5.7	0.8522	-1.5550	0.8983	-1.7094
								8.6	0.8522	-1.4175	0.8983	-1.6173

The values of Sf_x and Nu_x presented in Table 5 are obtained from the numerical solution of the governing equations using the shooting method. Specifically, these quantities correspond to the wall derivatives $f''(0)$ and $-\theta'(0)$, respectively. The variation in nanoparticle volume fractions φ_{Cu}, $\varphi_{Al_2O_3}$, φ_{MWCNT} influences the thermophysical properties of the fluid and consequently modifies the velocity and temperature gradients at the wall. These changes are reflected in the computed values of Sf_x and Nu_x.

Table 6: Energy transport rate of $Cu + Al_2O_3 + MWCNT\,/\,H_2O$

φ	**THNF**($Cu + Al_2O_3$ $+MWCNT\,/\,H_2O$) Nu_x	**HNF**($Cu + Al_2O_3$ $/H_2O$) Nu_x	**Enhancement %**
0.01	-1.8441	-1.8901	2.434
0.03	-1.6185	-1.7488	7.451
0.05	-1.4175	-1.6173	12.35
0.07	-1.2433	-1.4961	16.9
0.1	-1.0282	-1.3333	22.88
0.13	-0.8596	-1.1916	27.86
0.15	-0.7678	-1.1076	30.68
0.17	-0.6893	-1.0311	33.15
0.2	-0.5917	-0.9287	36.29

Table 6 presents the enhancement in energy transport rate for $Cu + Al_2O_3 + MWCNT\,/\,H_2O$. The values are taken when $m = 0.5$, $M = 1.5$, $R = 1$, $\Pr = 6.2$, $\gamma = 0.5$, $\varphi_{Cu} = \varphi_{Al_2O_3} = \varphi_{MWCNT} = 0.05, n = 8.6$. For THNF, all nanoparticle volume fractions $0.01 \leq \varphi_{Cu}, \varphi_{Al_2O_3}, \varphi_{MWCNT} \leq 0.2$. The computed Nusselt numbers reveal a significant enhancement in energy performance. It is observed that this THNF exhibits a 36.29% improvement in energy transmission compared to the hybrid nanofluid, a 59.30% enhancement over the nanofluid, and a significant 69.87% improvement when compared to base fluid. The enhancement in heat transfer is attributed to the combined effect of multiple nanoparticles, which improves the effective thermal conductivity and heat transfport capability of the fluid. The percentage enhancement in energy transmission rate is evaluated using:

$$\text{Enhancement } (\%) = \frac{(Nu_x)_{\text{THNF}} - (Nu_x)_{\text{HNF}}}{(Nu_x)_{\text{HNF}}} \times 100. \tag{26}$$

To demonstrate the computation of the enhancement percentage, consider the case when ($\varphi_{Cu} = \varphi_{Al_2O_3} = \varphi_{MWCNT} = 0.2$). From Table 6, the corresponding values of Nu_x are:
HNF ($Cu + Al_2O_3\,/\,H_2O$): -0.9287.
THNF($Cu + Al_2O_3 + MWCNT\,/\,H_2O$): -0.5917.
Using Eq. (22), the enhancement in heat transfer is calculated as:

$$\text{Enhancement } (\%) = \frac{-0.5917 - (-0.9287)}{-0.9287} \times 100 = 36.29\%.$$

The percentage enhancement is computed based on the absolute values of the Nusselt number.

5.1 Fuzzy analysis

This section compares the fuzzy curves of various nanoparticle shapes for THNF through $TriF_{number}$ and the $TrapF_{number}$. The nanoparticles volume fraction of THNF is considered as $TriF_{number}$ and analyzed using the α-cut approach ($0 \leq \alpha \leq 1$). The basic governing FDE's are transformed into lower and upper bounds with the help of the α-cut approach, and then solved numerically via the shooting technique.

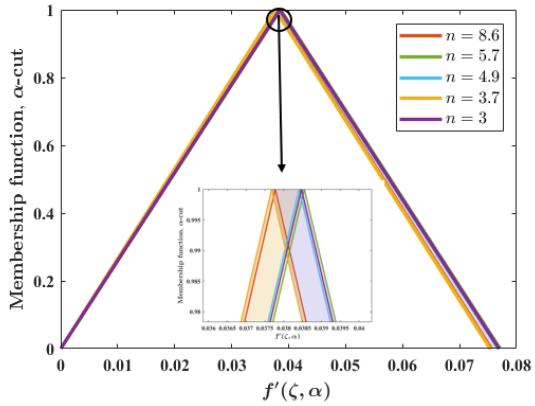

Figure 7: Fuzzy velocity at $\zeta = 0.5$ for various shape factors using $TriF_{number}$

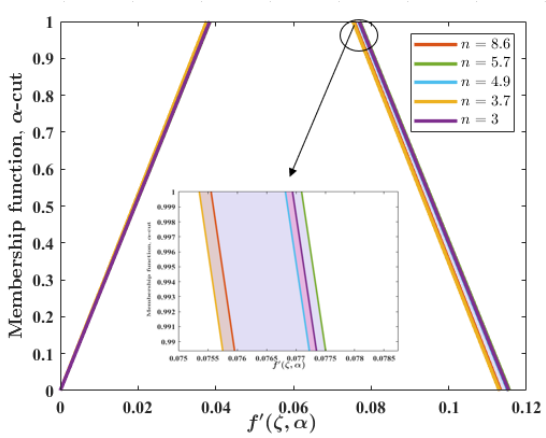

Figure 8: Fuzzy velocity at $\zeta = 0.5$ for various shape factors using $TrapF_{number}$

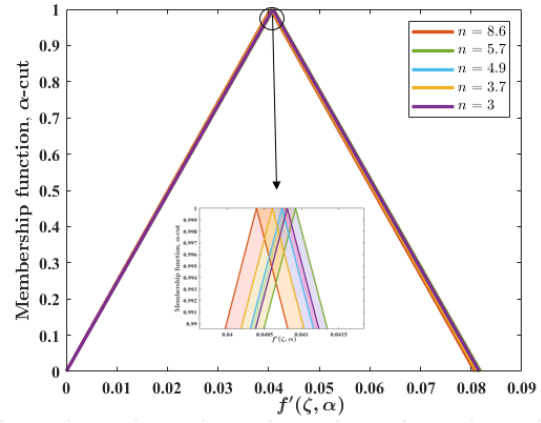

Figure 9: Fuzzy velocity at $\zeta = 1$ for various shape factors using $TriF_{number}$

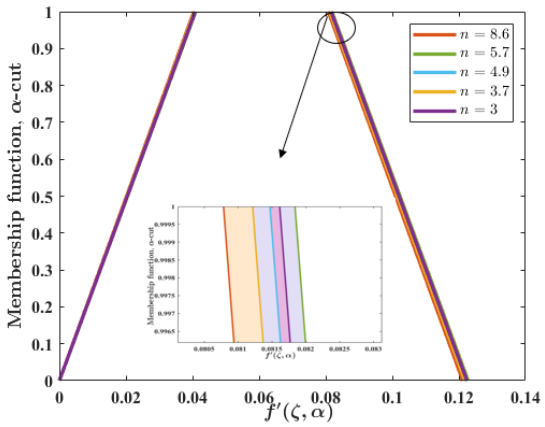

Figure 10: Fuzzy velocity at $\zeta = 1$ for various shape factors using $TrapF_{number}$

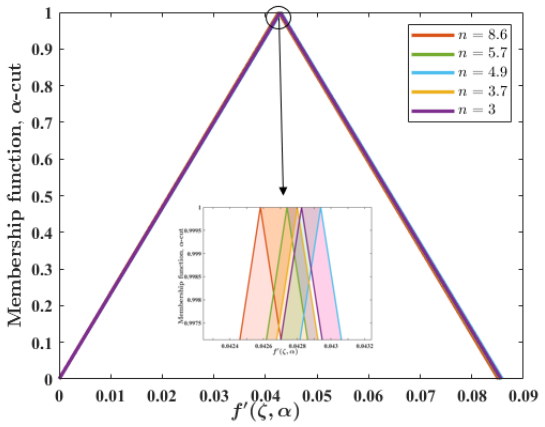

Figure 11: Fuzzy velocity at $\zeta = 1.5$ for various shape factors using $TriF_{number}$

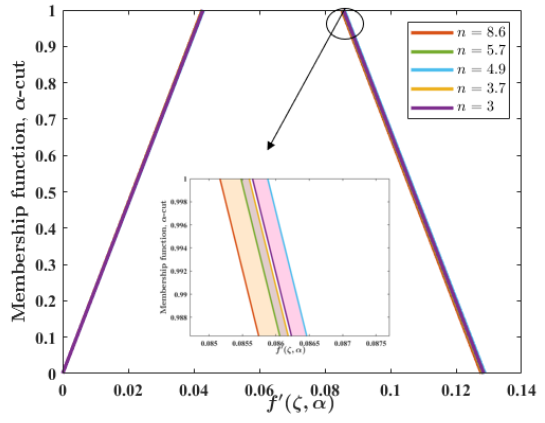

Figure 12: Fuzzy velocity at $\zeta = 1.5$ for various shape factors using $TrapF_{number}$

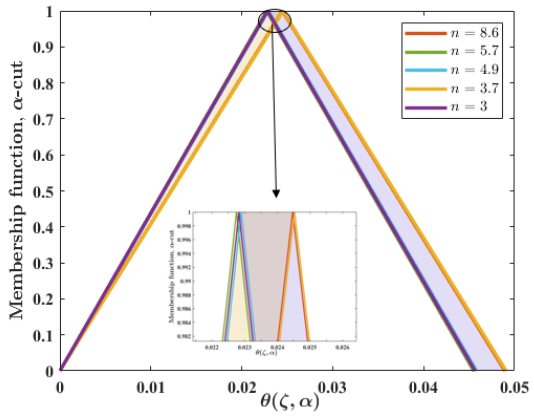

Figure 13: Fuzzy temperature at $\zeta = 0.5$ for various shape factors using $TriF_{number}$

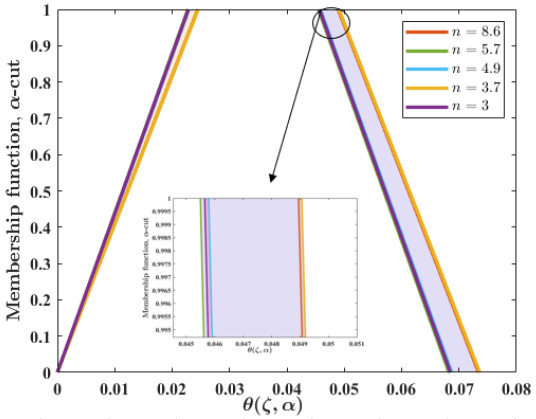

Figure 14: Fuzzy temperature at $\zeta = 0.5$ for various shape factors using $TrapF_{number}$

Figures 7, 8, 9, 10, 11, and 12 illustrate the fuzzy velocity curves by considering the volumetric fraction as a $TriF_{number}$ [0, 0.05, 0.1] and a $TrapF_{number}$ [0, 0.05, 0.1, 0.15] for different nanoparticle shapes at $\zeta = 0.5$,1,1.5. The vertical axis represents the fuzzy membership function at various α -cuts, while the horizontal axis shows the variation in $f''(\zeta)$. Although the volumetric fractions are modeled as symmetric $TriF_{number}$, the resulting fuzzy curves are not perfectly triangular symmetric. This asymmetry is due to the influence of the governing nonlinear equations. It is observed that blade-shaped nanoparticles display a wider spread compared to other nanoparticle shapes. Blade-shaped nanoparticles increase the viscosity and increase fluid resistance. Because of this, the velocity field becomes sensitive to small variations like changes in nanoparticle fraction, thermal effects, boundary effects. It is shows that uncertainty is greater than other nanoparticle shapes under both the $TriF_{number}$ and $TrapF_{number}$.

Figures 13, 14, 15, 16, 17, and 18 compare the fuzzy temperature curves for different nanoparticle shapes for THNF across various ζ values. In this analysis, THNF volume fractions are modeled as $TriF_{number}$ and $TrapF_{number}$, with $\varphi_{Cu}, \varphi_{Al_2O_3}$, and φ_{MWCNT} are taken as non-zero. The fuzzy temperature curves are plotted for different nanoparticle shape factors, with colors assigned as follows: red for $n = 8.6$, green for $n = 5.7$, blue for $n = 4.9$, orange for $n = 3.7$ and purple for $n = 3$. Blade-shaped nanoparticles show a wider spread than the other nanoparticle shapes. Blade-shaped nanoparticles have more intense contact with the base fluid, because they have a larger surface area compared to spherical or other shapes. This stronger interaction, even small changes in the volumetric fraction cause bigger effects in the system. So, the system causing larger uncertainty in the blade-shaped nanoparticle under both the $TriF_{number}$ and a $TrapF_{number}$.

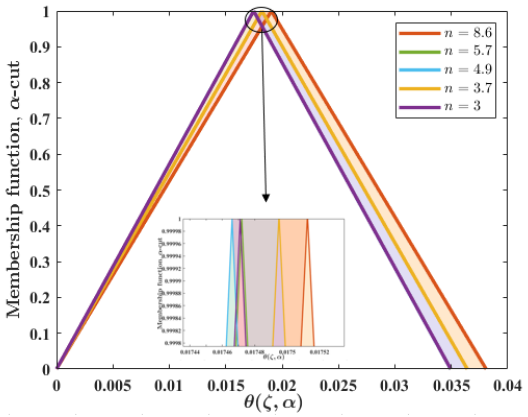

Figure 15: Fuzzy temperature at $\zeta = 1$ for various shape factors using $TriF_{number}$

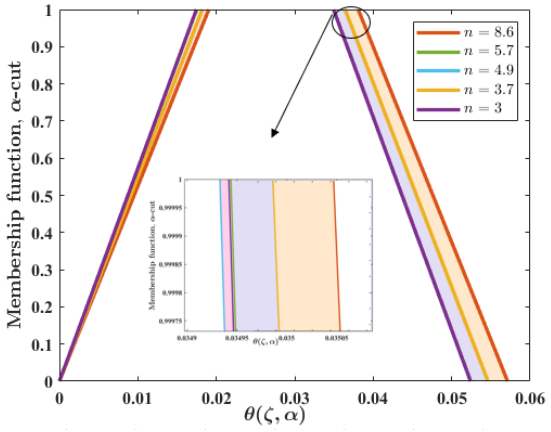

Figure 16: Fuzzy temperature at $\zeta = 1$ for various shape factors using $TrapF_{number}$

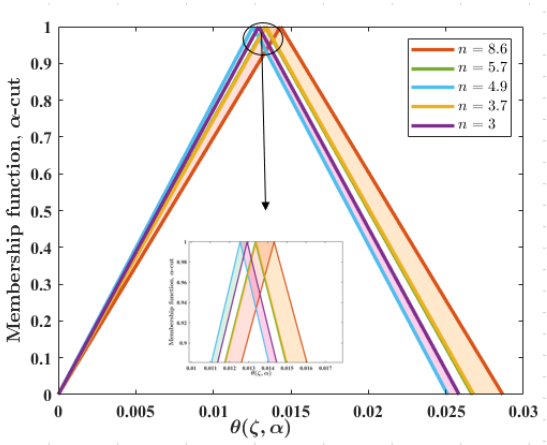

Figure 17: Fuzzy temperature at $\zeta = 1.5$ for various shape factors using $TriF_{number}$

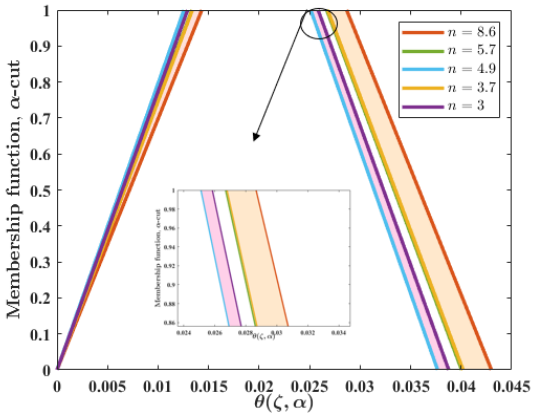

Figure 18: Fuzzy temperature at $\zeta = 1.5$ for various shape factors using $TrapF_{number}$

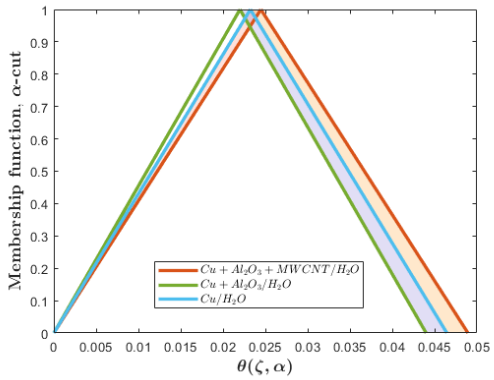

Figure 19: Comparison of THNF, HNF and NF Fuzzy temperature at $\zeta = 0.5$ using $TriF_{number}$

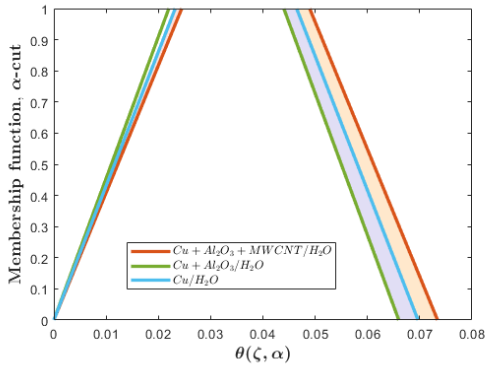

Figure 20: Comparison of THNF, HNF and NF Fuzzy temperature at $\zeta = 0.5$ using $TrapF_{number}$

In figures 19 and 20, the fuzzy temperature profiles of nanofluid, hybrid nanofluid and THNF for $n = 8.6$ are compared at $\zeta = 0.5$ using $TriF_{number}$ and a $TrapF_{number}$. The figure presents three scenarios. In the first scenario, φ_{Cu} is expressed as TriF and TrapF numbers and a $TrapF_{number}$ and is represented by blue lines. The second scenario corresponds to the HNF, where both φ_{Cu}, $\varphi_{Al_2O_3}$ are non zero and is represented by green lines. The third scenario represents the THNF, where φ_{Cu} and $\varphi_{Al_2O_3}$ and φ_{MWCNT} are non-zero and is represented by red lines. The results show that the THNF reaches a higher temperature than the NF and BF. This happens because the combined

Cu+Al_2O_3+$MWCNT$ nanoparticles allow heat to move more easily through the fluid, improving its overall thermal conductivity. As a result, the ternary hybrid nanofluid shows better thermal performance.

Table 7: Mean values of fuzzy data at $\zeta = 0.5$

Nanoparticle shapes	$TriF_{number}$		$TrapF_{number}$	
	Velocity	**Temperature**	**Velocity**	**Temperature**
Blade	0.0378	0.0245	0.0567	0.0367
Platelet	0.0379	0.0244	0.0565	0.0368
Cylinder	0.0385	0.0228	0.0578	0.0341
Brick	0.0385	0.0228	0.0577	0.0342
Sphere	0.0384	0.0229	0.0576	0.0343

Table 7 presents the mean values of fuzzy THNF a , expressed as TriF and TrapF numbers. It is observed that the triangular membership function has lower mean values than the trapezoidal membership function. This indicates that the triangular membership function captures a better possible value for all shapes. Therefore, the triangular fuzzy membership function gives more compact results while the trapezoidal fuzzy membership function leads to a wider variation.

6 Conclusions

The present study focused on the investigation of energy and mass transport in magnetized THNF ($Cu + Al_2O_3 + MWCNT \,/\, H_2O$) over a moving wedge under an uncertain environment. The influence of nanoparticle volume fractions φ_{Cu}, $\varphi_{Al_2O_3}$ and φ_{MWCNT} on the velocity, and temperature for THNF are analyzed. The nanooparticle volume fraction is considered as both $TriF_{number}$ and $TrapF_{number}$ with the help of the α-cut technique ($0 \leq \hat{\alpha} \leq 1$) to manage the fuzziness. The fuzzy differential equations (FDEs) are solved numerically using the MATLAB solver via the shooting method. The key outcomes of this study are summarized below:

- The combined effect of the Hartree pressure gradient (m) and magnetic field parameter (M) exhibits an increasing trend in $f''(0)$.
- The thermal radiation parameter (R), Prandtl number (Pr), and nanoparticle volume fraction (ϕ) show an increasing trend in $\theta'(0)$.
- THNF achieves a 36.29% higher heat transport rate compared to HNF, 59.30% higher than NF, and 69.87% higher than base fluid.
- The results obtained using the $TriF_{number}$ and $TrapF_{number}$ reveal that blade-shaped nanoparticles are more effective in enhancing the heat transport rate compared to other nanoparticle shapes.
- The triangular membership function yields a narrower uncertainty band compared to the trapezoidal membership function.

Limitations of the study

The present study is carried out under certain simplifying assumptions. The flow is considered steady, and some thermophysical properties are assumed to be constant. The analysis is restricted to a specific flow configuration over a moving wedge using similarity transformation. In addition, the uncertainity is introduced only through the nanoparticle volume fraction within a fuzzy framework, while other parameters are treated as deterministic.

Future scope

In the present study, ternary hybrid nanofluid flow over a moving wedge has been investigated within a fuzzy framework by incorporating uncertainty in the nanoparticle volume fraction. Future research can extend this model to bio-based tetra-hybrid nanofluids by including nanoparticle shape effects, variable thermophysical properties, and additional physical mechanisms such as porous medium, viscous dissipation, and activation energy effects. Moreover, alternative numerical approaches and comparative analyses may be considered to further validate and improve the results.

Acknowledgment

The authors extend their sincere gratitude to the Management, Principal, Sri Sivasubramaniya Nadar College of Engineering, Chennai, India.

Declarations

- Author contributions
  Conceptualization, M.S.P.; methodology, M.S.P., B. A., and R.S.W.; software, M.S.P., and B. A.; validation, M.S.P., and B. A.; formal analysis, M.S.P., R.S.W.; investigation, M.S.P., and B. A.; data curation, M.S.P., B. A., and R.S.W.; writing-initial draft formulation, M.S.P., and B. A.; writing-review and refinement, M.S.P., R.S.W., and S.B; visual representation, M.S.P., and B. A.; guidance, M.S.P., R.S.W., and S.B; All authors have reviewed and approved the final version of the manuscript.
- Funding
  This research did not receive financial support from external sources.
- Data availability
  The data generated in this study are available from the corresponding author upon reasonable request.
- Competing interests
  The authors have no conflicts of interest to disclose.
- Ethical approval
  This article does not involve any studies with human or animal subjects.

References

[1] M. Abbas, N. Khan, M. S. Hashmi, Z. Salleh, H. Ullah, A. S. Alsubaie, S. Rezapour, M. Inc, *Numerical simulation of Darcy-Forchheimer flow of Casson ternary hybrid nanofluid with melting phenomena and local thermal non-equilibrium effects*, Case Studies in Thermal Engineering, **60** (2024), 104694. https://doi.org/10.1016/j.csite.2024.104694

[2] H. AL Garalleh, *Numerical simulation of heat transport mechanism in chemically influenced ternary hybrid nanofluid flow over a wedge geometry*, Discover Applied Sciences, **6**(9) (2024), 449. https://doi.org/10.1007/s42452-024-06141-4

[3] A. M. Alqahtani, W. Khan, F. Smarandache, N. Becheikh, R. Alroobaea, T. Muhammad, *Numerical solution of hybrid nanofluid and its stability over permeable wedge sheet with heat transfer analysis*, IEEE Access, **12** (2024), 57633-57645. https://doi.org/10.1109/ACCESS.2024.3378513

[4] A. A. Al-Saedi, L. Verma, R. Meher, O. Nikan, *Study on Jeffery-Hamel nano-fluid flow with uncertain volume fraction using semi-analytical approach*, AIP Advances, **15**(4) (2025). https://doi.org/10.1063/5.0268586

[5] N. Amar, N. Kishan, *The influence of radiation on MHD boundary layer flow past a nano fluid wedge embedded in porous media*, Partial Differential Equations in Applied Mathematics, **4** (2021), 100082. https://doi.org/10.1016/j.padiff.2021.100082

[6] A. Ayub, S. Z. H. Shah, Z. Sabir, A. Rashid, M. R. Ali, *A novel study of the Cross nanofluid with the effects of inclined magnetic field in fuzzy environment*, International Journal of Thermofluids, **22** (2024), 100636. https://doi.org/10.1016/j.ijft.2024.100636

[7] A. A. Azar, P. Jalili, Z. P. Moziraji, B. Jalili, D. D. Ganji, *Analytical solution for MHD nanofluid flow over a porous wedge with melting heat transfer*, Heliyon, **10**(15) (2024). https://doi.org/10.1016/j.heliyon.2024.e34888

[8] A. Chakraborty, R. Saadeh, A. Qazza, N. Zomot, P. Janapatla, U. Khan, T. Muhammad, *On the thermal performance of radiative stagnation-point hybrid nanofluid flow across a wedge with heat source/sink effects and sensitivity analysis*, Frontiers in Materials, **11** (2024), 1391377. https://doi.org/10.3389/fmats.2024.1391377

[9] S. S. Chang, L. A. Zadeh, *On fuzzy mapping and control*, IEEE Transactions on Systems, Man, and Cybernetics, **SMC-2**(1) (1972), 30-34. https://doi.org/10.1109/TSMC.1972.5408553

[10] S. U. Choi, J. A. Eastman, *Enhancing thermal conductivity of fluids with nanoparticles*, Argonne National Lab (ANL), Argonne, IL (United States), 1995.

[11] S. Choudhary, V. Kumar Jarwal, P. Choudhary, K. Loganathan, B. Pattanaik, *Mass-based hybrid nanofluid model for thermal radiation analysis of MHD flow over a wedge embedded in porous medium*, Journal of Engineering, **2024**(1) (2024), 9528362. https://doi.org/10.1155/2024/9528362

[12] N. Deepa, P. Kavya, N. Thamaraikannan, S. Madhanraj, P. Asaigeethan, K. Loganathan, *Fuzzy volume fraction model representation of blood-based Sisko Tri-hybrid nanofluid flow via a non-linear stretching cylinder*, International Journal of Thermofluids, **29** (2025), 101354. https://doi.org/10.1016/j.ijft.2025.101354

[13] D. Dubois, H. Prade, *Operations on fuzzy numbers*, International Journal of Systems Science, **9**(6) (1978), 613-626. https://doi.org/10.1080/00207727808941724

[14] M. Faizan, M. Ajithkumar, M. V. Reddy, M. A. Jamal, B. Almutair, N. A. Shah, J. D. Chung, *A theoretical analysis of the ternary hybrid nano-fluid with Williamson fluid model*, Ain Shams Engineering Journal, **15**(8) (2024), 102839. https://doi.org/10.1016/j.asej.2024.102839

[15] U. Farooq, M. Imran, N. Fatima, *Computational insights into the thermal behavior of SWCNT-Fe3O4 and MWCNT-CuO hybrid nanofluids in stretching cylinder with response surface methodology*, Multiscale and Multidisciplinary Modeling, Experiments and Design, **8**(4) (2025), 221. https://doi.org/10.1007/s41939-025-00786-3

[16] W. Ibrahim, A. Tulu, *Magnetohydrodynamic (MHD) boundary layer flow past a wedge with heat transfer and viscous effects of nanofluid embedded in porous media*, Mathematical Problems in Engineering, **2019**(1) (2019), 4507852. https://doi.org/10.1155/2019/4507852

[17] K. Jabeen, M. Mushtaq, M. Akram, *Suction and injection impacts on Casson nanofluid with gyrotactic microorganisms over a moving wedge*, Journal of Fluids Engineering, **144**(1) (2022), 011204. https://doi.org/10.1115/1.4051484

[18] B. Jalili, P. M. Zar, D. Liu, C. H. Ji, P. Jalili, M. A. Abdelmohimen, D. D. Ganji, *Thermal study of MHD hybrid nano fluids confined between two parallel sheets: Shape factors analysis*, Case Studies in Thermal Engineering, **63** (2024), 105229. https://doi.org/10.1016/j.csite.2024.105229

[19] S. Khalil, T. Abbas, R. Nawaz, *Enhanced thermal and flow behavior of Cu-Al2O3/water hybrid nanofluids in porous media under variable magnetic field conditions*, International Journal of Thermofluids, **27** (2025), 101166. https://doi.org/10.1016/j.ijft.2025.101166

[20] S. A. Khan, M. Imran, H. Waqas, T. Muhammad, S. Yasmin, A. Alhushaybari, *Numerical analysis of multiple slip effects on CuO/MgO/TiO2-water ternary hybrid nanofluid with thermal and exponential space-based heat source*, Tribology International, **197** (2024), 109778. https://doi.org/10.1016/j.triboint.2024.109778

[21] W. A. Khan, I. Pop, *Boundary layer flow past a wedge moving in a nanofluid*, Mathematical Problems in Engineering, **2013**(3) (2013), 637285. https://doi.org/10.1155/2013/637285

[22] S. G. Krishna, M. Shanmugapriya, *Inquiry of MHD bioconvective non-newtonian nanofluid flow over a moving wedge using HPM*, Materials Today: Proceedings, **38**(5) (2021), 3297-3305. https://doi.org/10.1016/j.matpr.2020.10.028

[23] A. Kumar, R. Meher, *Study on uncertain impact of thermal radiation on micropolar hybrid nanofluid flow between porous channel walls with distinct nanoparticles*, Journal of Taibah University for Science, **18**(1) (2024), 2352008. https://doi.org/10.1080/16583655.2024.2352008

[24] H. Masuda, A. Ebata, K. Teramae, N. Hishinuma, *Alteration of thermal conductivity and viscosity of liquid by dispersing ultra-fine particles. Dispersion of Al2O3, SiO2 and TiO2 ultra-fine particles*, Netsu Bussei, **7**(4) (1993), 227-233. https://doi.org/10.2963/jjtp.7.227

[25] J. C. Maxwell, *A treatise on electricity and magnetism*, Oxford: Clarendon Press, **1** (1873).

[26] P. Mishra, M. R. Acharya, S. Panda, *Mixed convection MHD nanofluid flow over a wedge with temperature-dependent heat source*, Pramana, **95** (2021), 1-12. https://doi.org/10.1007/s12043-021-02087-z

[27] T. Pathinathan, K. Ponnivalavan, E. M. Dison, *Different types of fuzzy numbers and certain properties*, Journal of Computer and Mathematical Sciences, **6**(11) (2015), 631-651.

[28] S. S. K. Raju, P. Durgaprasad, J. L. D. Palencia, A. Wakif, et. al., *Contour analysis for heat transfer rate in a wedge geometry with non-uniform shapes nanofluid: Gradient descent machine learning technique*, Results in Engineering, **23** (2024), 102714. https://doi.org/10.1016/j.rineng.2024.102714

[29] C. S. K. Raju, M. M. Hoque, T. Sivasankar, *Radiative flow of Casson fluid over a moving wedge filled with gyrotactic microorganisms*, Advanced Powder Technology, **28**(2) (2017), 575-583. https://doi.org/10.1016/j.apt.2016.10.026

[30] S. Rao, P. N. Deka, *Numerical analysis of MHD hybrid nanofluid flow a porous stretching sheet with thermal radiation*, International Journal of Applied and Computational Mathematics, **10**(3) (2024), 95. https://doi.org/10.1007/s40819-024-01734-4

[31] M. V. Reddy, A. Moorthi, S. A. Lone, F. Ali, et. al., *Magneto-Williamson nanofluid flow past a wedge with activation energy: Buongiorno model*, Advances in Mechanical Engineering, **16**(1) (2024), 1-10. https://doi.org/10.1177/16878132231223027

[32] M. Shanmugapriya, R. Sundareswaran, S. G. Krishna, M. Pal, *An analysis of effect of higher order endothermic/exothermic chemical reaction on magnetized casson hybrid nanofluid flow using fuzzy triangular number*, Engineering Applications of Artificial Intelligence, **133**(B) (2024), 108119. https://doi.org/10.1016/j.engappai.2024.108119

[33] M. Shanmugapriya, R. Sundareswaran, P. S. Kumar, G. Rangasamy, *Impact of nanoparticle shape in enhancing heat transfer of magnetized ternary hybrid nanofluid*, Sustainable Energy Technologies and Assessments, **53**(C) (2022), 102700. https://doi.org/10.1016/j.seta.2022.102700

[34] K. Varatharaj, R. Tamizharasi, K. Vajravelu, *Ternary hybrid nanofluid flow and heat transfer at a permeable stretching sheet with slip boundary conditions*, The European Physical Journal Special Topics, **234**(8) (2025), 2293-2316. https://doi.org/10.1140/epjs/s11734-024-01295-z

[35] N. A. Yacob, A. Ishak, I. Pop, *Falkner-Skan problem for a static or moving wedge in nanofluids*, International Journal of Thermal Sciences, **50**(2) (2011), 133-139. https://doi.org/10.1016/j.ijthermalsci.2010.10.008

[36] L. A. Zadeh, *Fuzzy sets*, Information and Control, **8**(3) (1965), 338-353. https://doi.org/10.1016/S0019-9958(65)90241-X

[37] N. A. Zainal, I. Waini, N. S. Khashi'ie, R. Nazar, I. Pop, *MHD hybrid nanofluid flow past a stretching/shrinking wedge with heat generation/absorption impact*, CFD Letters, **16**(6) (2024), 146-156. https://doi.org/10.37934/cfd.16.6.146156

[38] A. Zeeshan, D. Hussain, Z. Asghar, M. M. Bhatti, F. Z. Duraihem, *Thermal optimization of MHD nanofluid over a wedge by using response surface methodology: Sensitivity analysis*, Propulsion and Power Research, **12**(4) (2023), 556-567. https://doi.org/10.1016/j.jppr.2023.10.003

[39] R. M. Zulqarnain, M. Nadeem, I. Siddique, H. Ahmad, S. Askar, M. Samar, *Heat transfer analysis of Maxwell tri-hybridized nanofluid through Riga wedge with fuzzy volume fraction*, Scientific Reports, **13**(1) (2023), 18238. https://doi.org/10.1038/s41598-023-45286-x